

Kuhn, T., et al., 2017, Widespread seawater circulation in 18–22 Ma oceanic crust: Impact on heat flow and sediment geochemistry: *Geology*, doi:10.1130/G39091.1

FIGURE CAPTIONS SUPPLEMENTARY DATA

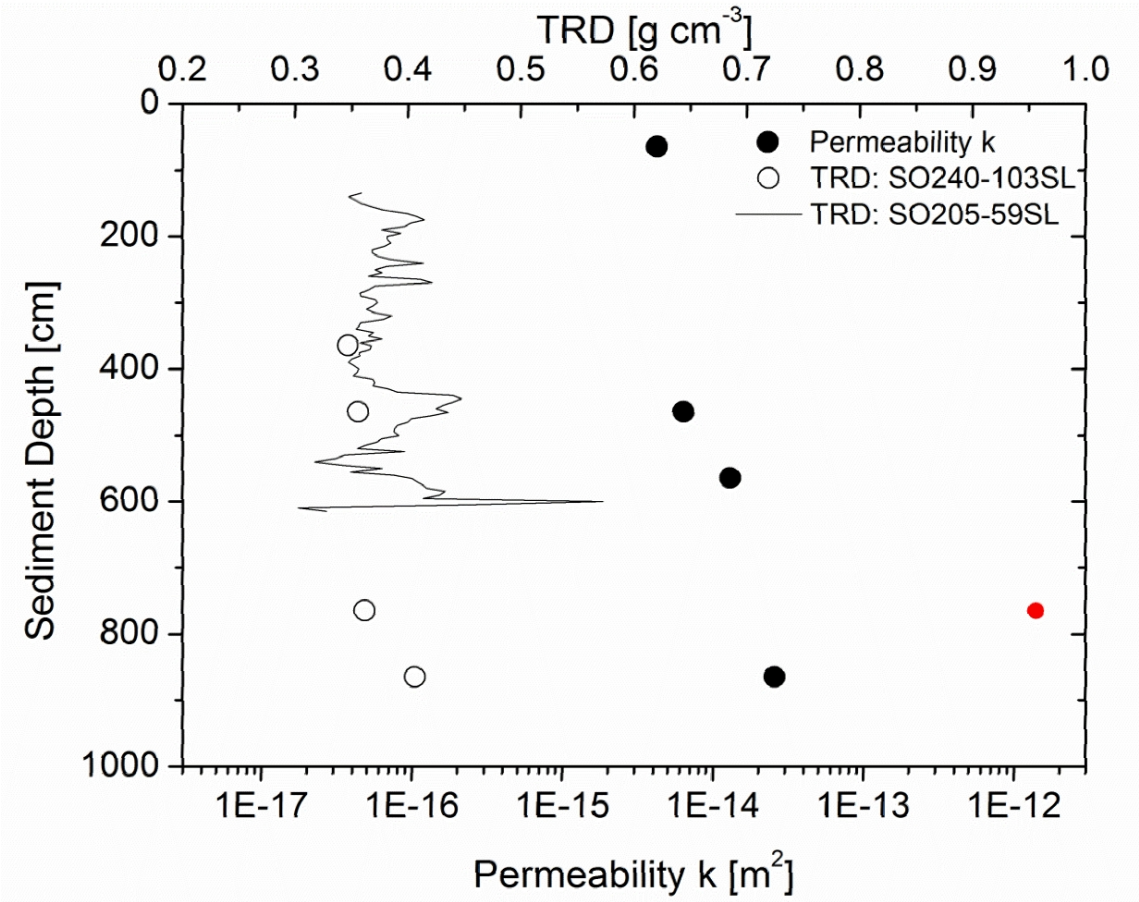
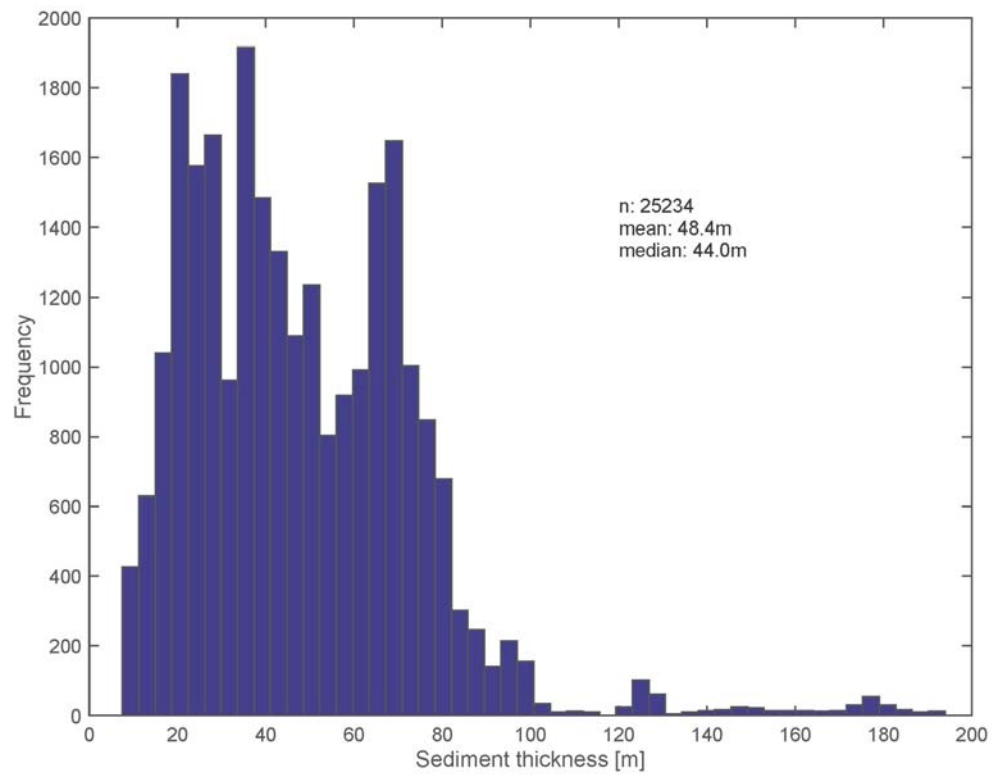


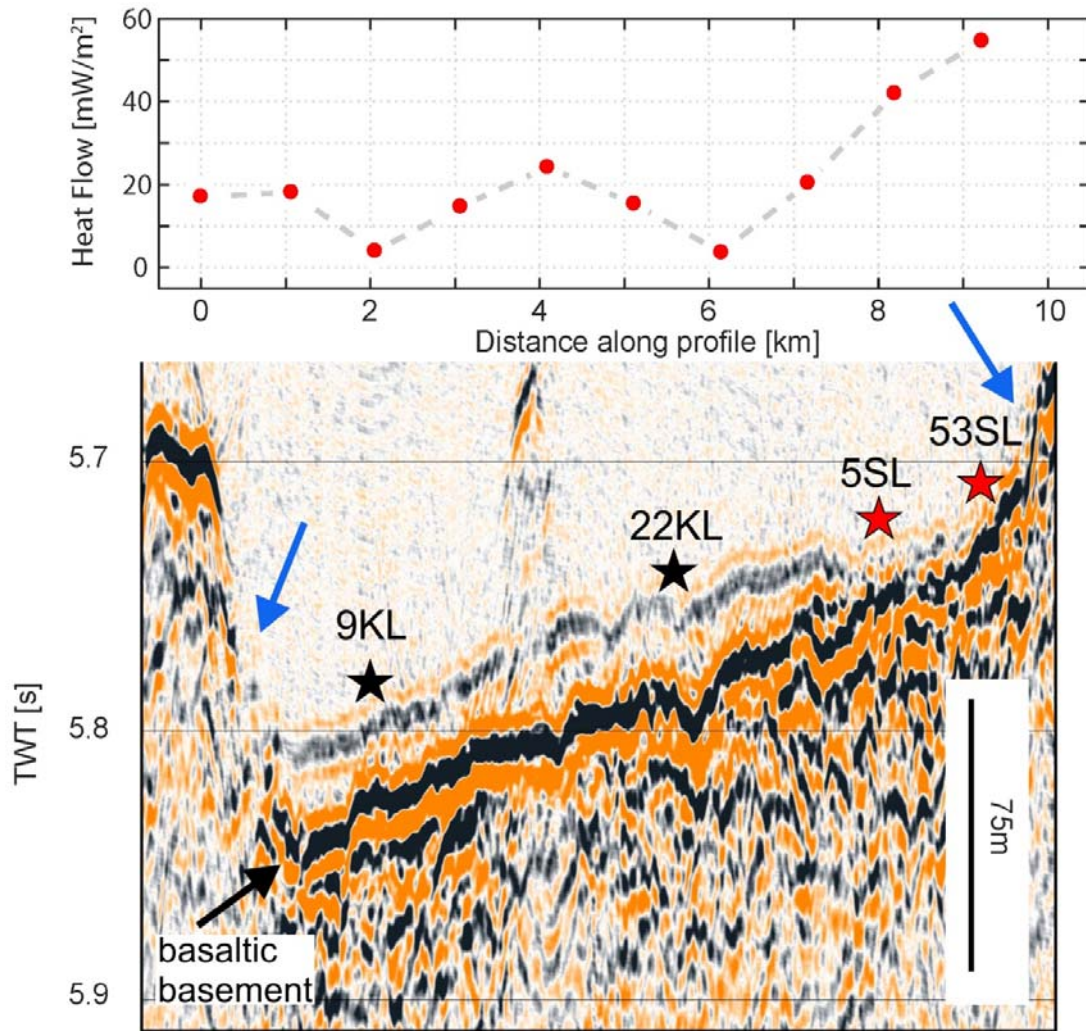
Figure DR1: Permeability versus depth in sediment core 103SL as well as dry bulk density of this core and of core SO205/59SL from the same working area for comparison (Rühlemann et al., 2010).



8

9 Figure DR2: Histogram of the sediment thickness detected along the seismic lines run during  
 10 SO240 with a mean thickness of 48 m. The “picked sediment thickness” is based on a few  
 11 seismic lines in the working area but we are confident that they give a realistic impression  
 12 on the sediment thickness in general.

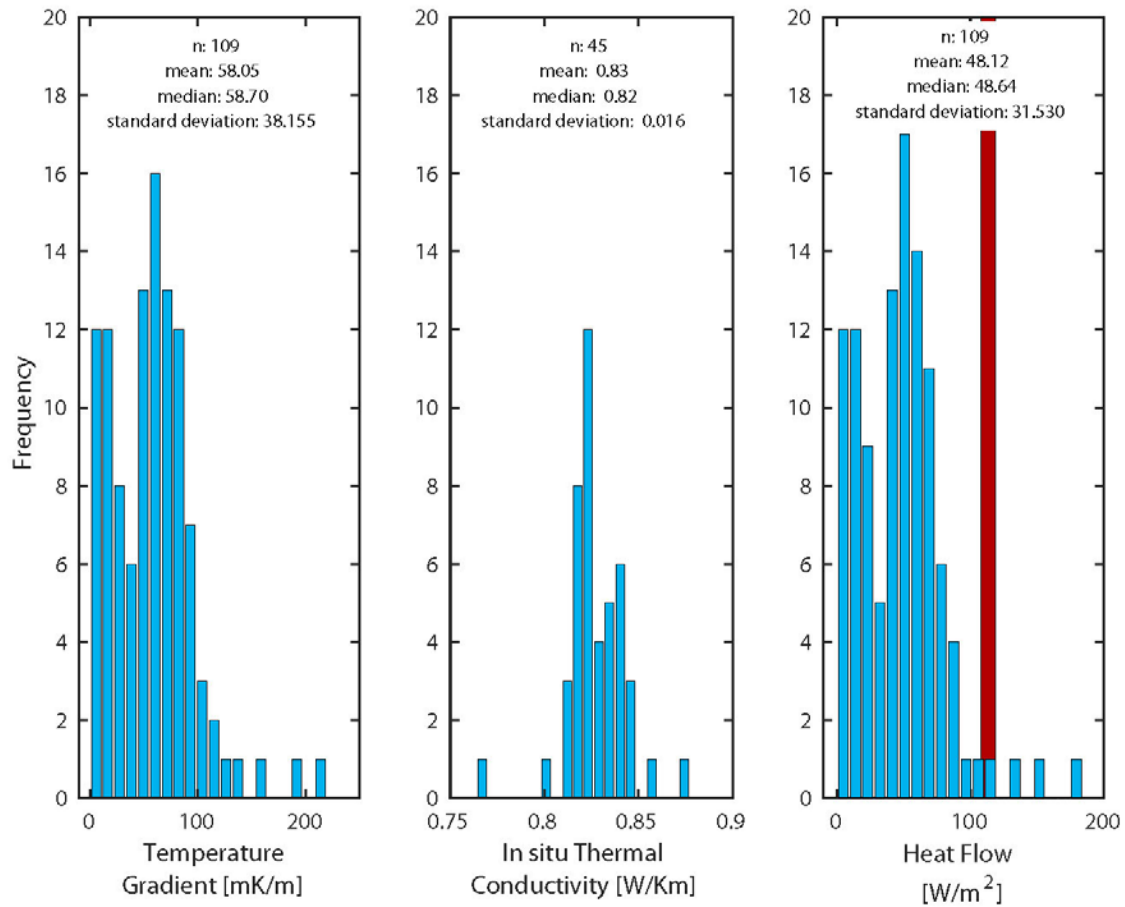
13



14

15 Figure DR3: Seismic profile and heat flow values at the locations of sediment cores 9KL,  
 16 22KL, 5SL, and 53SL east of the Teddy Bare seamount (see Fig. 1 for location). Red stars  
 17 mark sediment cores which are oxic throughout, black stars mark cores which are suboxic at  
 18 depth. Note the increasing sediment thickness from E to W. Blue arrows indicate  
 19 outcropping basaltic crust where seawater may recharge and discharge. Seawater may  
 20 laterally flow in the basalts underneath the sediments.

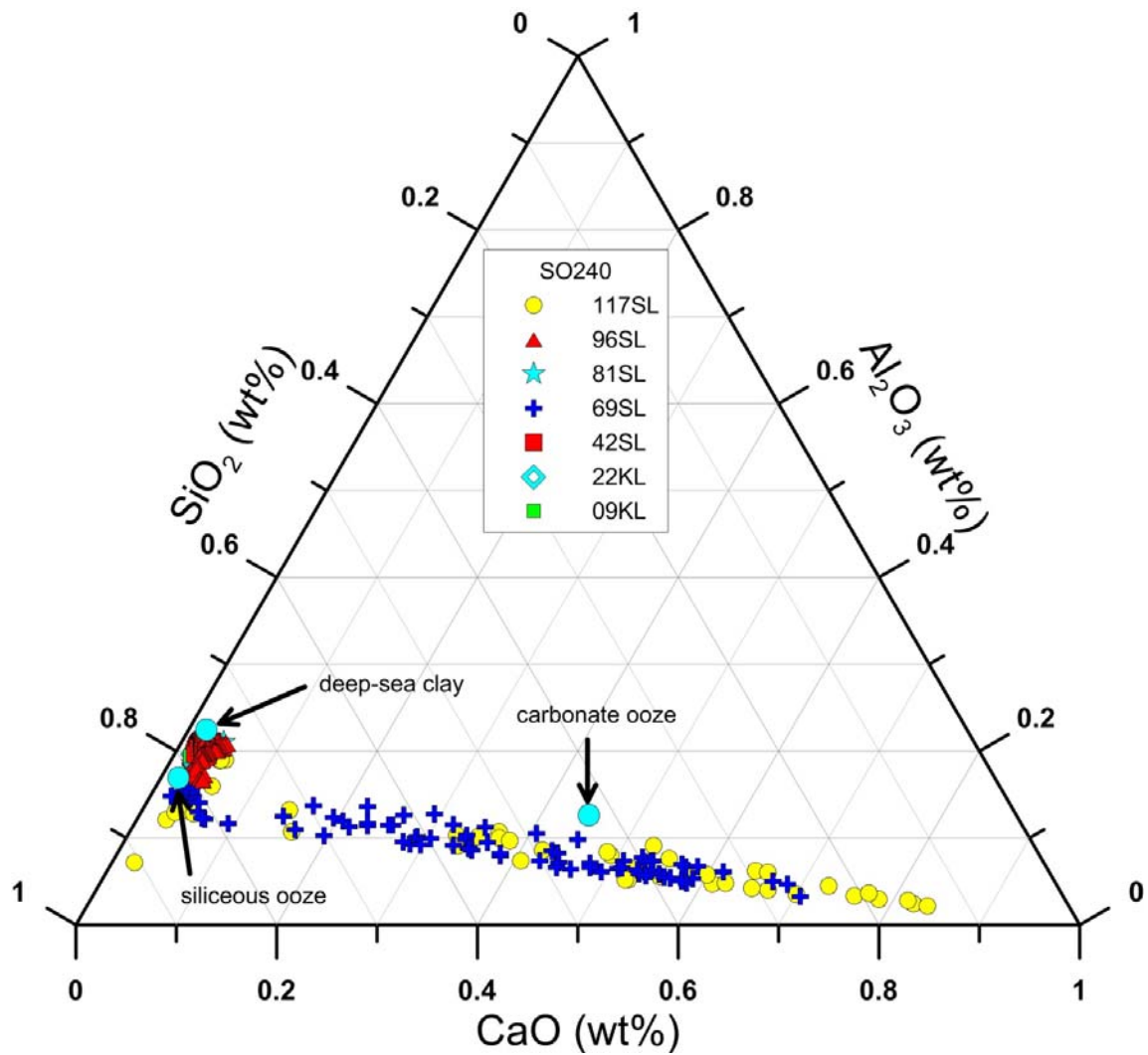
21



22

23 Figure DR4: Compilation of all in-situ measured heat flow and conductivity data as well as  
 24 the calculated temperature gradient (see Kuhn et al., 2015). The red column marks the heat  
 25 flow from lithospheric conductive cooling predictions which is between ~108 and 119  
 26 mW/m<sup>2</sup> for 18 to 22 Ma old oceanic crust (Hasterock, 2013).

27



28

29 Figure DR5:  $\text{SiO}_2$ - $\text{CaO}$ - $\text{Al}_2\text{O}_3$  ternary diagram of sediments from seven sites in the working  
 30 area (N=755; XRF data, analyses at BGR). Note that all sediments from stations 09, 22, 42,  
 31 81, and 96 are mixtures between siliceous ooze and deep-sea clay, whereas the deep parts of  
 32 cores 69SL and 117SL contain significant fractions of carbonate. Literature data are average  
 33 values from Chester (2000; Table 13.3, 13.4).

34

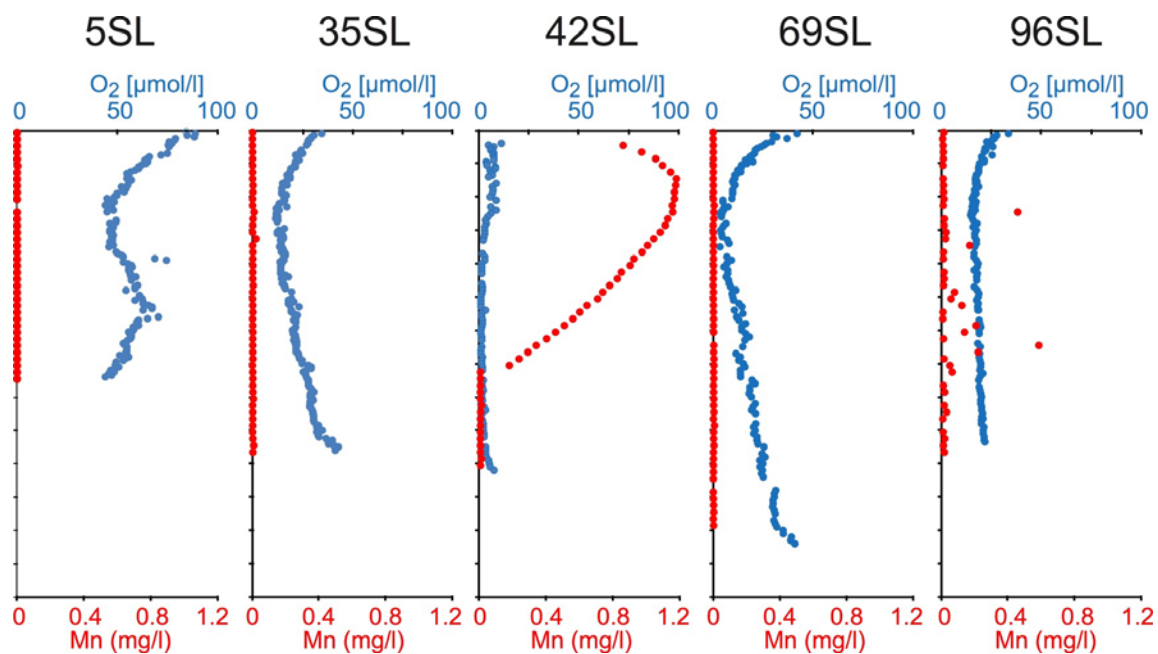
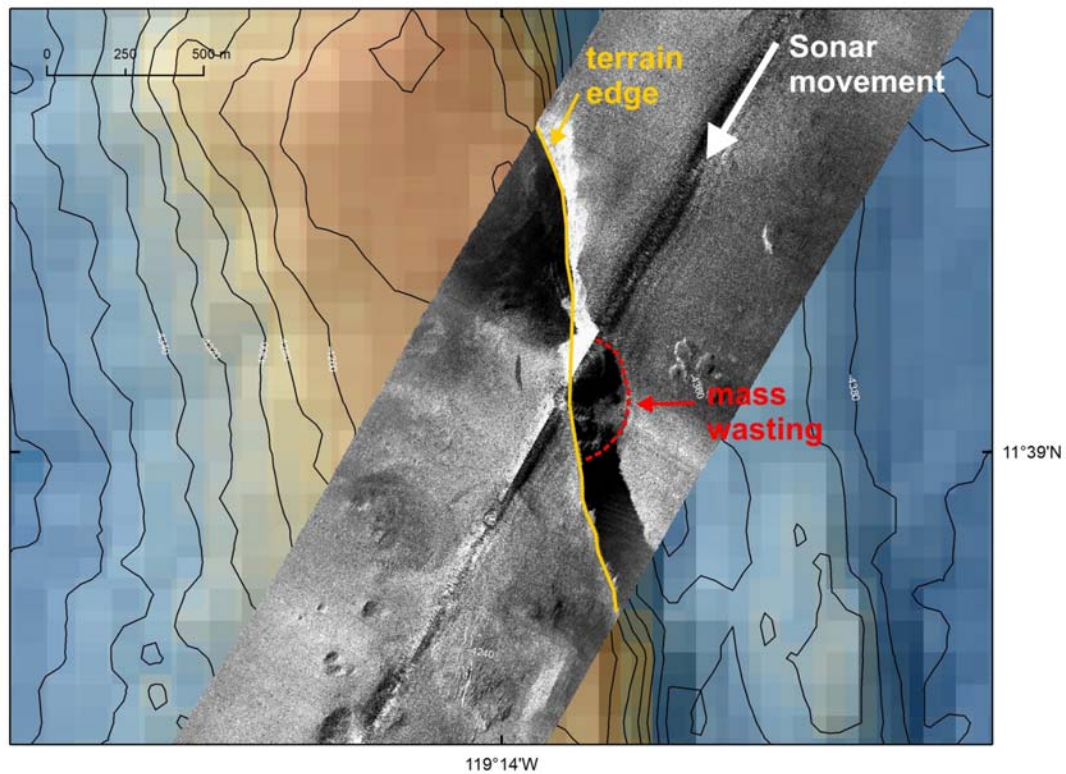


Figure DR6: Pore-water concentration profiles of O<sub>2</sub> and Mn<sup>2+</sup> for sediment cores not shown in the main article. See Figure 1 of the main article for location of cores.





39

40 Figure DR7: Side-scan sonar track on top of the bathymetry over a N-S oriented ridge. Side-  
 41 scan data are presented as 8-bit grey values with white colour indicating high backscatter.  
 42 Vehicle movement (IMI-120A from University of Hawaii) was from NE to SW during  
 43 cruise MANGAN-2009 with R/V Kilo Moana (Wiedicke-Hombach et al., 2010). Strong  
 44 white area facing towards the vehicle during by-pass on its lower side is interpreted as  
 45 vertical cliff running parallel to the bathymetric ridge. This cliff forms shadows when the  
 46 vehicle passes it from the top side. High backscatter suggest outcropping hard rocks. Height  
 47 of the cliff is 80 – 100 m.

48

49   **REFERENCES** (not cited in the main article)

50   Chester, R., 2000, Marine Geochemistry, Wiley-Blackwell, 520 pp.

51   Rühlemann, C. and Shipboard Scientific Party, 2010, Microbiology, Paleoceanography and

52        Biodiversity in the Manganese Nodule Belt of the Equatorial NE Pacific, Cruise Report

53        SO205/MAGAN: Hannover, Germany, 112 p.

54   Wiedicke-Hombach, M. and Shipboard Scientific Party, 2010, Campaign to the German

55        Contract Area for Polymetallic Nodule Exploration (RV Kilo Moana Cruise MANGAN-

56        2009), Hannover, 64 pp.



TABLE DR1. PISTON (KL) AND GRAVITY (SL) CORER LOCATIONS OF THIS STUDY

| Corer ID | Location  |            | Water depth (m) | Corer length (m) | Recovery (cm) | O <sub>2</sub> at base | Sediment cover (m) | Fault |
|----------|-----------|------------|-----------------|------------------|---------------|------------------------|--------------------|-------|
|          | Lat (°N)  | Long (°W)  |                 |                  |               |                        |                    |       |
| 05SL     | 13°10.53' | 118°06.71' | 4287            | 10               | 756           | Yes                    | <10                | Yes   |
| 09KL     | 13°10.52' | 118°10.10' | 4335            | 15               | 1187          | No                     | 23                 | No    |
| 22KL     | 13°10.53' | 118°07.66' | 4319            | 15               | 1161          | No                     | 22                 | ?     |
| 35SL     | 12°54.13' | 118°24.79' | 4319            | 10               | 982           | Yes                    | 18                 | No    |
| 53SL     | 13°10.51' | 118°06.11' | 4273            | 5                | 482           | Yes                    | <10                | No    |
| 69SL     | 12°39.86' | 119°13.37' | 4275            | 15               | 1265          | Yes                    | 51                 | Yes   |
| 81SL     | 11°50.06' | 116°32.89' | 4355            | 15               | 1346          | Yes                    | 73                 | Yes   |
| 103SL    | 11°49.25' | 117°03.85' | 4137            | 15               | 977           | ---                    | 37                 | Yes   |
| 108SL    | 11°48.80' | 116°31.77' | 4326            | 15               | 1038          | No                     | 20                 | No    |
| 117SL    | 13°11.10' | 118°05.99' | 4271            | 15               | 600           | Yes                    | <10                | No    |